RSC Advances

Carbon supported Fe-Co nanoparticles with enhanced activity and BH4− tolerant used as a cathode in passive air breathing anion exchange membrane direct borohydride fuel cell

Journal:	*RSC Advances*
Manuscript ID:	RA-ART-10-2014-012857.R1
Article Type:	Paper
Date Submitted by the Author:	04-Feb-2015
Complete List of Authors:	ZHiani, Mohammad; Isfahan University of Technology, Chemistry Mohammadi, Ismaeil; Isfahan University of Technology,, Chemistry Salehi Najafabadi, Nafiseh; Isfahan University of Technology, Chemistry

RSC Advances

RSC Publishing

Paper

Carbon supported Fe-Co nanoparticles with enhanced activity and BH_4^- tolerant used as a cathode in passive air breathing anion exchange membrane direct borohydride fuel cell

Cite this: DOI: 10.1039/x0xx00000x

Received 00th January 2012,
Accepted 00th January 2012

DOI: 10.1039/x0xx00000x

www.rsc.org/

M. Zhiani,*[a] I. Mohammadi[a] and N. Salehi[a]

The performance and borohydride-tolerance of a non-noble metal cathode nano-catalyst, Hypermec^{TM}K14, were investigated in an anion-exchange membrane direct borohydride fuel cell (DBFC). Cell polarization curves in passive air breathing DBFC indicate that the DBFC equipped with non-noble metal cathode catalyst exhibit higher open circuit voltage and peak power density compared to the DBFC which uses commercial 10 wt. % Pt/C in the cathode side; 0.970 V and 138 mW cm^{-2} vs 0.752 V and 48 mW cm^{-2}. Data on the performance of active DBFC using Hypermec^{TM}K14 gives power densities of 890 mW cm^{-2} using oxidant and fuel flow rate 250 and 6 $mlmin^{-1}$ respectively at 75°C. Further electrochemical investigations were done by a driven-cell mode in order to compare the $NaBH_4$- tolerance of Hypermec^{TM}K14 and 10 wt. % Pt/C in DBFC. Hypermec^{TM}K14 exhibits excellent tolerance toward $NaBH_4$ electrooxidation compared to 10 wt. % Pt/C catalyst; 10 times higher according to the produced current density form oxidation of crossed-over fuel. Separation of anode and cathode polarizations in both membrane electrode assemblies (MEAs) confirms that the difference in the cathode polarizations is responsible for the difference in the obtained cell power densities. Electrochemical impedance spectra of both cells also demonstrate lower charge and mass transfer resistances for DBFC equipped by Hypermec^{TM}K14, which is consistent with the obtained performance. Catalyst layers microstructure was also investigated by N_2 adsorption (BET) and scanning electron microscopy (SEM).

Introduction

Hydrogen-fuel based proton exchange membrane fuel cells (PEMFCs) have been improved substantially as promising alternative power sources for transportation and mobile applications due to their high-energy efficiency and fast start-up. However, their successful commercialization is restricted by the safety, supply, storage efficiency, transportation of their flammable gas fuel and high stack cost. Accordingly, certain liquid fuels such as methanol, ethanol, glycerol etc. have been considered for fueling PEMFCs directly. However, slow anodic kinetics, toxicity, fuel crossover and low theoretical voltages inhibit the performance of these organic fuels. Therefore, sodium borohydride as a promising hydrogen-carrying liquid fuel has attracted considerable attention due to its many advantageous features: high theoretical open circuit voltage (1.64V), high H-capacity, faster anodic electrooxidation rate, more compact cell structure compared to direct alcohol fuel cells, and more convenient fuel storage and handling than the conventional H_2-based fuel cells. The high capacity of 5.67 Ahg^{-1}, the high theoretical energy conversion rate (91%) and the large number of transferred electrons are the other advantageous features of sodium borohydride[2-82-82-82-82-8]. The direct borohydride fuel cell is based on the borohydride ion oxidation and the oxygen reduction to release 8e- according to the following reactions:

Anode: $BH_4^- + 8OH^- \rightarrow BO_2^- + 6H_2O + 8e^-$
$E^0_{anode} = -1.24V$ vs. SHE (1)
Cathode: $O_2 + 2H_2O + 4e^- \rightarrow 4OH^-$
$E^0_{cathode} = 0.4V$ vs. SHE (2)
Overall: $BH_4^- + 2O_2 \rightarrow BO_2^- + 2H_2O$
$E^0_{cell} = 1.64V$ vs. SHE (3)

Nevertheless, depending on the electrode material, the eight-electron borohydride oxidation may compete with the quasi-spontaneous heterogeneous hydrolysis of reaction (4) at the electrode.[9]

$BH_4^- + 2H_2O \rightarrow BO_2^- + 2\,H_2$ (4)

In principle, DBFCs can only work in an alkaline environment because borohydride may suffer spontaneous reaction with

water for pH<12.[10] Alkaline fuel cells, including DBFC, possess two special advantages over the PEMFC: (i) kinetics of electrodes in alkaline media is faster than acid media; (ii) it is possible to use low cost non-noble electrocatalysts and support materials without detrimental electro-kinetic performance and stability losses. Nevertheless, the development of alkaline fuel cells (AFCs) was hindered by the carbonation of electrolyte due to CO_2 production resulting from the fuel oxidation and air as well. CO_2 carbonation with alkaline electrolyte has been a main challenge since the early days of AFC development. However, the resurgence of AFCs is due to recent advances in solid anion exchange membranes (AEMs) technology[11] because the carbonation is largely reduced by using the AEMs as the electrolyte. However, hydrogen evolution (reaction 4) is another major obstacle to commercial DBFC development. This reaction lowers DBFC columbic efficiencies and produces bubbles on the surface of electrode. The latter can cause mechanical failure and safety issues in DBFC.[12] The other significant trouble in the development of the DBFC is BH_4^--crossover from anode side to the cathode side. The fuel crossover deteriorates the open circuit voltage (OCV) and cathode performance, causing the decline of the power density. On the other hand, the effect of fuel crossover on cell and cathode performance strongly depends on the cathode material.[13] In order to overcome this problem, exploring new cathode catalysts which have high tolerance to fuel oxidation and low cost as well, without sacrificing catalyst activity, has been the main concern and the subject of numerous investigations in recent years.[14]

Using alkaline media for stabilizing $NaBH_4$ offers the possibility of using non- platinum cathode catalysts. Research into a wide range of cathode catalysts such as Pt/C, Au/C, Ag/C, Pd/C and Ni/C has been conducted by H. Cheng et. al..[6] A major concern in using Pt/C for commercial applications is its high cost. Moreover, Pt/C, Ag/C and Au/C exhibit electrocatalytic activity towards BH_4^- oxidation; therefore, they are not suitable for using as a cathode catalyst.[15] Ni cathode catalyst is also instable. Other possible kinds of oxide catalysts such as MnO_2/C[16] and Eu_2O_3 demonstrate noticeable electrochemical activity for oxygen reduction reaction (ORR) as well as good borohydride tolerance; however, their final performance is not satisfactory.[17] Furthermore, several transition-metal macrocyclic compounds including iron tetramethoxyphenyl porphyrin (FeTMPP),[18] Cobalt Phthalocyanin,[19] Iron Phthalocyanin/C,[20] Co-PPY-C[21] and amorphous Fe-based catalyst composed of amorphous FeOOH and microcrystalline Fe_2O_3 supported on polypyrrole modified carbon nanotubes (CNTs)[22] have been developed and successfully applied as cathode catalysts in DBFCs.

Perovskite-type oxides were also used as cathode in DBFC.[14, 23-26] They indicated good activity and stability in the ORR.

Nevertheless, a further study is required to address the commercialization of non-noble, ORR-active, borohydride-tolerant and durable cathode catalysts for DBFC application.

The aim of the present work was to assay non-platinum low-cost cathode catalyst, Fe-Co Hypermec^{TM}K14, for ORR and BH_4^--tolerance measurement in alkaline DBFC. A few groups have successfully employed Hypermec^{TM}K14 as a cathode catalyst in alkaline direct alcohol fuel cells.[27-30] In this study, Hypermec^{TM}K14 was investigated for the first time in a direct borohydride fuel cell. The performance and electrochemical behavior of Hypermec^{TM}K14 were evaluated and compared to the commercial 10 wt. % Pt/C catalysts in DBFC by i-V curves and EIS. Comparison of the cathodes polarization was carried out and discussed by separating anode and cathode polarizations of both MEAs containing Hypermec^{TM}K14 and 10 wt. % Pt/C. BH_4^--tolerance of both catalysts was measured using driven-cell mode in a single passive DBFC. Data on the performance of active DBFC under identical catalysts condition are also reported. Morphological characterizations of the cathode catalysts were also studied by field emission scanning electron microscopy (FE-SEM) and SEM techniques.

Results and discussion

Morphological and physical characterization

SEM images of Hypermec^{TM}K14 and Pt/C microstructure were presented at different magnifications in Figure 1 and Figure 2, respectively. Figure 1a, indicates that a wide range of Hypermec^{TM}K14 agglomerations size, typically as a granular porous microstructure which did not uniformly disperse on the surface of the carbon cloth. A great number of pores and cracks appeared on the catalyst layer leading a high surface area and porosity available in the electrode. This morphology could be related to the ink preparation procedure, catalyst coating process and the catalyst and support specifications. Moreover, high-magnification image (Figure 1b) exhibited the details of the agglomerated particles size, macro and micro pores on the surface of the catalyst layer.

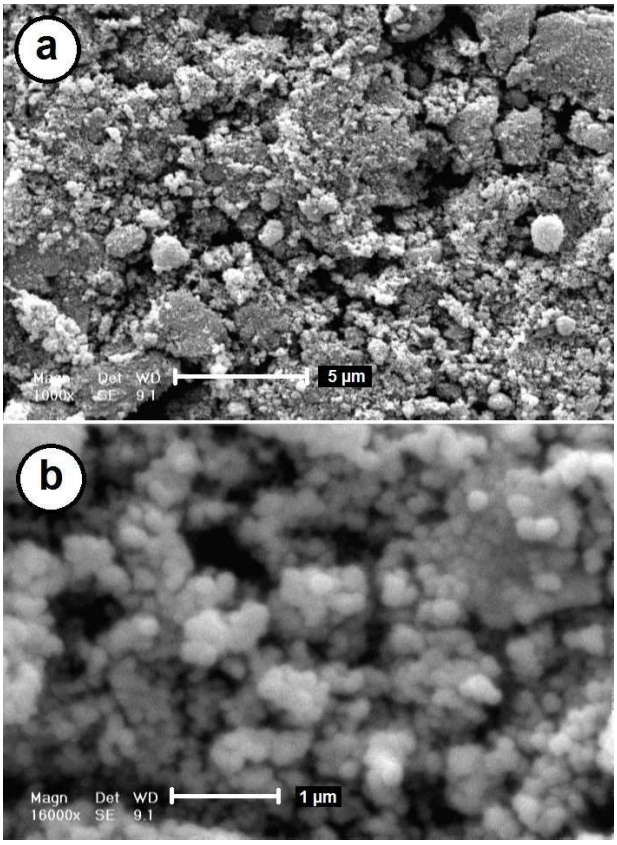

Figure 1 Different-magnification SEM images of Hypermec^{TM}K14.

Figure 2a and b, exhibits that Pt/C nanoparticles have a uniform dispersion on the carbon cloth, typically as a granular dense microstructure. The size of the agglomerated particles in Figure 1a is also lower than the Figure 2b.

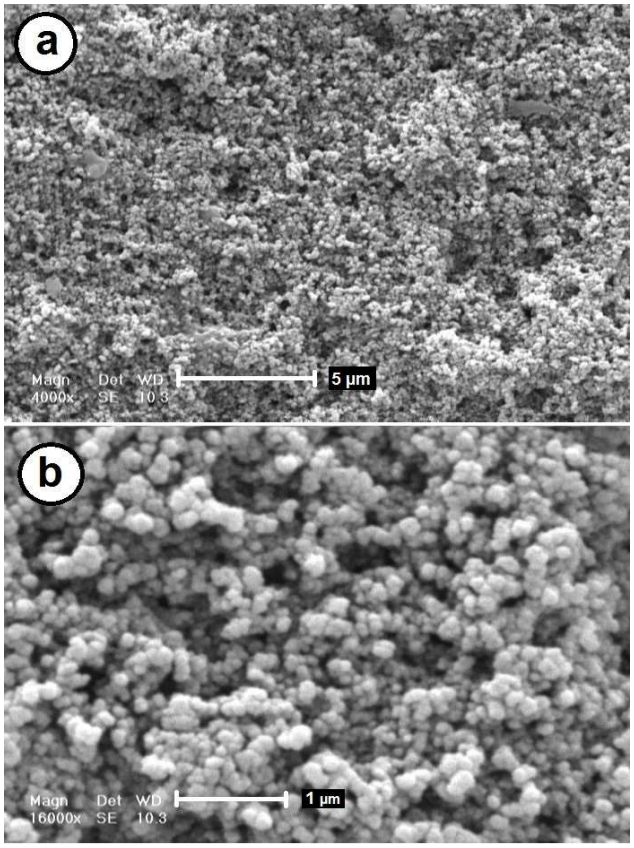

Figure 2. Different-magnification SEM images of 10 wt. % Pt/C

Table 1 presents Brunauer Emmett Teller (BET) specific surface area of both catalysts as determined by N_2 adsorption/desorption experiment. This table indicates that the surface area of the Hypermec^{TM}K14 and Pt/C is 542.447 and 212.172 m^2 gr^{-1} respectively. The higher surface area of the Hypermec^{TM}K14 could be related to the catalysts support specification; Ketjen carbon black (1200 m^2g^{-1}) vs. Vulcan XC 72 (250 m^2g^{-1}).

Table 1: BET Specific Surface Area of Pt/C and Hypermec^{TM}K14 catalyst sample

Sample	Specific BET surface area / m^2 g^{-1}
Pt/C	212.172
Hypermec^{TM}K14	542.447

Electrochemical characterization

Single cell performance

The polarization and power density curves of two DBFCs, with Hypermec^{TM}K14 cathode catalyst (denoted as MEA-K14) and 10 wt. % Pt/C cathode catalyst (denoted as MEA-Pt), have been presented in Figure 3a and Figure 3b respectively. According to Nernst equation (Eq. 5), the relationship between anode potential and electrolyte solution is shown by:

$$E=E^{\theta}+\frac{RT}{8F}\ln\frac{a_{OH^-}^{8}\times a_{BH_4^-}}{a_{H_2O}^{6}\times a_{BO_2^-}} \quad (5)$$

According to the above equation, the anode potential is determined by BH_4^- and OH^- ions activities.

By increasing BH_4^- concentration, the mass transfer of the fuel and the kinetics of borohydride oxidation would be improved, leading to higher power density; however, the fuel crossover and hydrolysis would also increase, resulting to lower open circuit voltage. The theoretical open circuit voltage of a DBFC is 1.64V. The actual cell voltage lowered to 1V. One reason is due to the crossover of sodium borohydride (SBH) from anode side to the cathode side. Another reason is the over-potential of the anode reaction, which will be discussed in next section. Therefore, there would be an optimized $NaBH_4$ concentration for better cell performance.[31] As can be seen in Figure 3, the DBFCs performance was improved with increasing sodium borohydride concentration from 1 wt. % to 5 wt. %. However, further increase in sodium borohydride concentration to 8 wt. % caused a decrease in the power density due to the enhancement of the fuel crossover and borohydride hydrolysis by increasing borohydride concentration. As the hydrolysis reaction proceeds, not only hydrogen bubbles are generated from catalyst surface, but also borate is formed. Hydrogen bubbles destruct the catalyst layer and mass transport of the reactant is substantially hindered by borate molecules. Table 2 indicates the performance analysis of both cells at ambient temperatures and pressures.

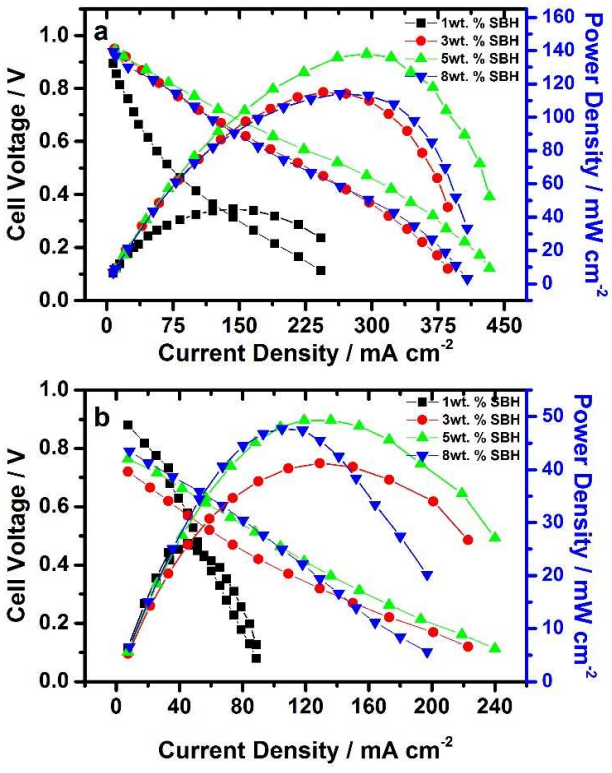

Figure 3. Cell polarization curves of (a) Hypermec^{TM}K14 and (b) 10 wt. % Pt/C in passive DBFCs fuelled by solution containing 1, 3, 5, and 8 wt. % of SBH.

Table 2. Performance analysis of MEA-K14 and MEA-Pt in air-breathing passive DBFCs fuelled by solution containing 5 wt. % SBH

i@0.7V $mAcm^{-2}$	i@0.5V $mAcm^{-2}$	i@0.2V $mAcm^{-2}$	MPD $mWcm^{-2}$	R mΩ	OCV mV	MEA
132	267.6	401.8	138	74	970	K14
29	91.1	187.8	48	87.9	752	Pt

Figure 4 shows the polarization and power density curves of the DBFC with MEA-K14 and MEA-Pt in 5 wt. % SBH. The OCV of the MEA-K14 is 0.970 V, which is 0.218 V higher than MEA-Pt (0.752 V). In addition, the peak power density of the MEA-K14 was 138mW cm^{-2}, which is 187% higher than MEA-Pt (48mW cm^{-2}). These results can be attributed not only to superior selectivity and activity of transition metal based Hypermec^{TM}K14 cathode catalyst toward ORR, but also to feeble catalytic activity towards electro-oxidation of crossed over sodium borohydride (a stronger tolerance to BH_4^- than 10 wt. % Pt/C catalyst). Another reason for high activity of Iron Cobalt catalysts was introduce by H. Tributsch.[32] They found that Fe/Co catalyst is a molecular multi-electron transfer catalyst and not one operating via catalytic nanoparticles as is the case of the platinum oxygen reduction catalyst.

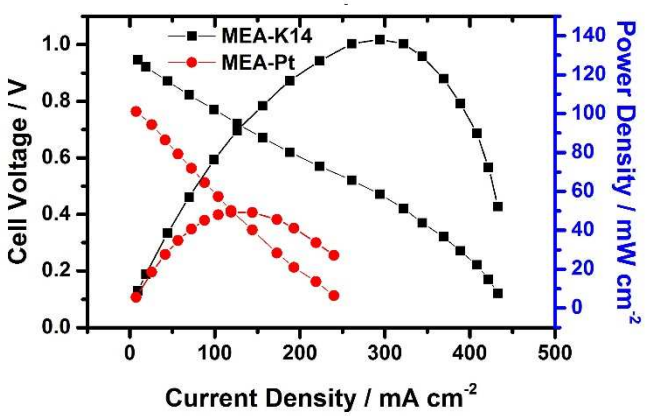

Figure 4. Comparison between cell polarization curves of Hypermec^{TM}K14 and 10 wt. % Pt/C in air-breathing passive DBFCs fuelled with 5 wt. % of SBH.

In order to study the cell polarizations in more details, the anode and cathode polarizations were separated by employing pseudo Zn/ZnO reference electrode.

Figure 5 shows the separated anode and cathode polarization curves of both MEAs in different sodium borohydride concentrations. The anode polarization of MEA-K14 are roughly identical to those of MEA-Pt, indicating that the cathodic materials, which allow us to conduct cathode kinetic comparative study, do not affect by the electro- oxidation of BH_4^- on the anode. However, the cathodes polarization differed significantly. The large variation in the cathodes polarization is noteworthy, confirming that the variation in cathode activity is responsible for different power densities seen in Figure 4. MEA-K14 has lower polarization losses than MEA-Pt, thereby demonstrating that Hypermec^{TM}K14 possess a notable activity for ORR in alkaline medium. As shown in Figure 5, the cathodic open-circuit voltage of MEA-K14 is highly different from MEA-Pt and the difference is increased with the enhancement of the fuel concentration. These values are lower than the standard value for the reduction of oxygen due to the mixed potential between crossed over borohydride ions and oxygen on the cathode side.[33] These results clearly show that by increasing the SBH concentration, BH_4^--crossover is accelerated upon the electrochemical oxidation of borohydride. Furthermore, there is an abrupt drop in the cell voltage starting from the open circuit voltage. This abrupt voltage drop in the electrode kinetic region of the polarization curve (current densities below 100 mA cm^{-2}) is due to the formation of a mixed potential on the cathode surface, which is because of crossed over borohydride ions.

Moreover, separation of anode and cathode polarizations in both MEAs demonstrate when the current density changes from 0 to 200 mA cm^{-2}, the anode over-potential increases from 0.27 to 0.54 V, while the cathode over-potential decreases from 1.24 to 1.15 V and 1.04 V to 0.74 V for MEA-K14 and MEA-Pt, respectively. These results demonstrate that the electrochemical dynamics of the anode is dramatically inferior to that of the cathode, and probably it is a main reason for low OCV in the Pd based anode DBFC.

Catalysts Borohydride Tolerate Measurement in DBFC

Due to the crossover of borohydride through the anion-exchange membrane from the anode side to the cathode side in DBFC, borohydride could be oxidized electrochemically on the cathode side depending on the typical cathode catalyst. Driven-cell mode tests were employed to characterize the borohydride tolerance determination of the cathode catalysts. Driven-cell mode tests were conducted in single DBFC by employing a pseudo Zn/ZnO reference electrode at the anode side, whilst anode was used as the counter electrode. The cathode of the DBFC was used as working electrode and N_2 gas was purged in the cathode side. the results indicate that with increasing SBH concentration in the anode side, more SBH oxidation current is observed, which is related to increasing of the borohydride crossover from the anode side to the cathode side. Figure 6 shows the driven-cell mode curves of both MEAs in a 10 wt. % KOH solution containing sodium borohydride with various concentrations.

The SBH oxidation current density is increased with increasing SBH concentration from 1 wt. % to 8 wt. %. It means the BH_4^--crossover is increased with the enhancement of the sodium borohydride concentration, especially on the cathode made by Pt/C 10wt. % (Figure 6b). For better comparison of borohydride tolerant of the two cathodes (MEA-K14 and MEA-Pt), driven-cell mode results in 5 wt. % SBH was presented in Figure.7.

As shown in Fig. 7, the onset potential for borohydride oxidation on the MEA-K14 shifted to more positive potentials. The borohydride oxidation current density on the MEA-K14 was several times less than the MEA-Pt, implying a strong tolerance of the Hypermec^{TM}K14 catalyst to BH_4^-.

More details on these results were examined by cyclic voltammetry (CV) technique in three electrodic half-cell compartments.

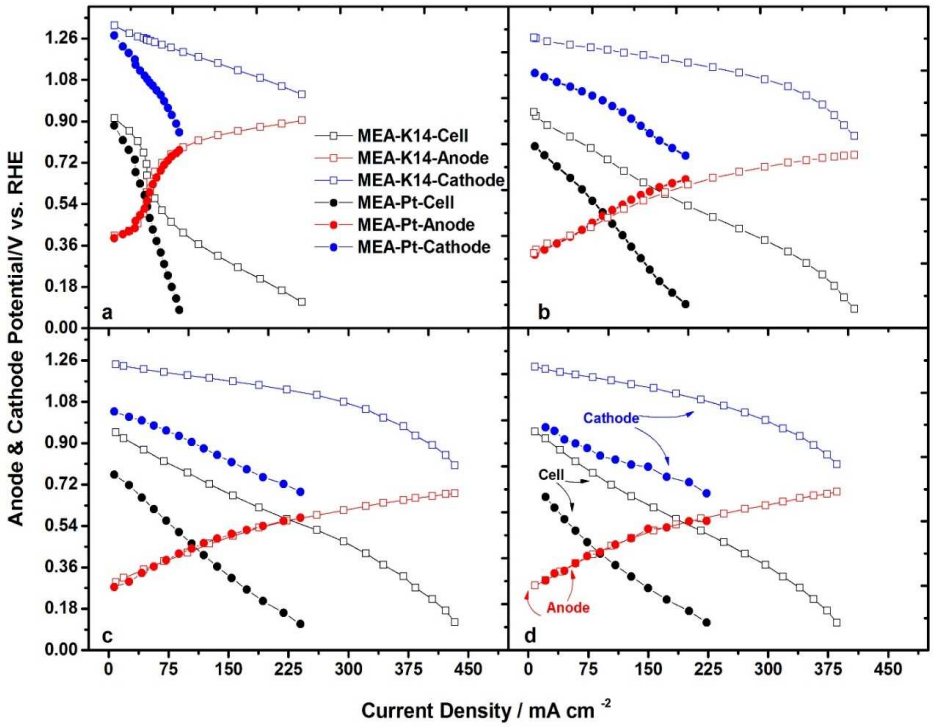

Figure 5. Anode, cathode and cell polarization curves of Hypermec^{TM}K14 and 10 wt. % Pt/C in air-breathing passive DBFCs fuelled by solution containing a) 1 wt. %, b) 3 wt. %, C) 5 wt. % and d) 8 wt. % of SBH

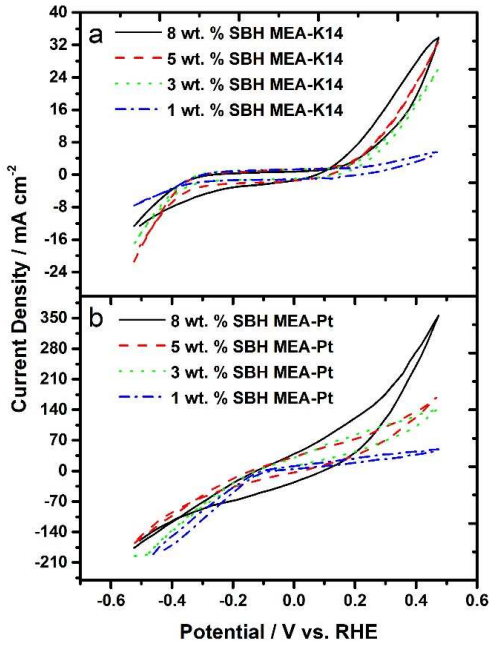

Figure 6. The oxidation current density of crossed-over BH_4^- on the (a) Hypermec^{TM}K14 and (b) 10 wt. % Pt/C in driven-cell mode with alkaline fuel containing 1, 3, 5, and 8 wt. % of SBH.

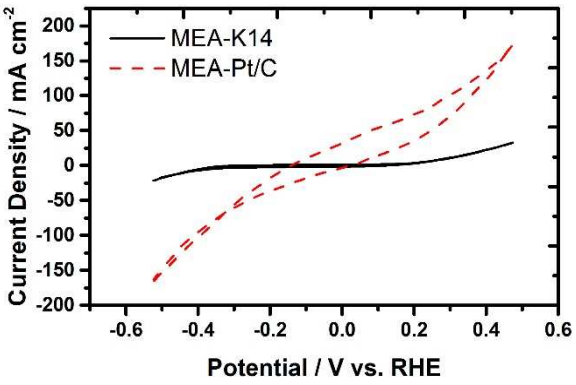

Figure 7. BH_4^--crossover measurement of Hypermec^{TM}K14 and 10 wt. % Pt/C in driven-cell mode fed by 5 wt. % of SBH.

Figure 8a shows the cyclic voltammogram of Hypermec^{TM}K14 loaded on glassy carbon (GC) in a freshly prepared 2 M KOH solution pre-purged with N_2, compared with that obtained for commercial Pt/C under identical conditions.

This figure indicates the Hypermec^{TM}K14 has a superior activity in oxygen reduction reaction compared to 10 wt. % Pt/C in alkaline media as it demonstrated by rotating disc electrode (RDE) technique in our previous article[27],

Therefore higher OCV could be achieved by MEA-K14, as it can be observed in Figure 4 and 5.

The cyclic voltammetry of the BH_4^- oxidation reaction on the Hypermec^{TM}K14 and Pt/C catalysts in a solution containing 50 mM $NaBH_4$ and 2M KOH under static condition is shown in Figure 8b. Comparison of the BH_4^- oxidation process on both catalysts indicates that the Hypermec^{TM}K14 has lower activity toward BH_4^- oxidation reaction compared to 10 wt. % Pt/C; 3.3 mA cm^{-2} vs. 44.3 mA cm^{-2} at -0.6V. This is an expectable result, because it is well know that Pt is an active catalyst for BH_4^- oxidation reaction and its hydrolysis compared to other catalyst.[34]

These result clearly indicate that the Hypermec^{TM}K14 is not sensitive toward the BH_4^- oxidation. In fact, it shows a remarkable selectivity to oxygen reduction reaction and inertness to borohydride oxidation.

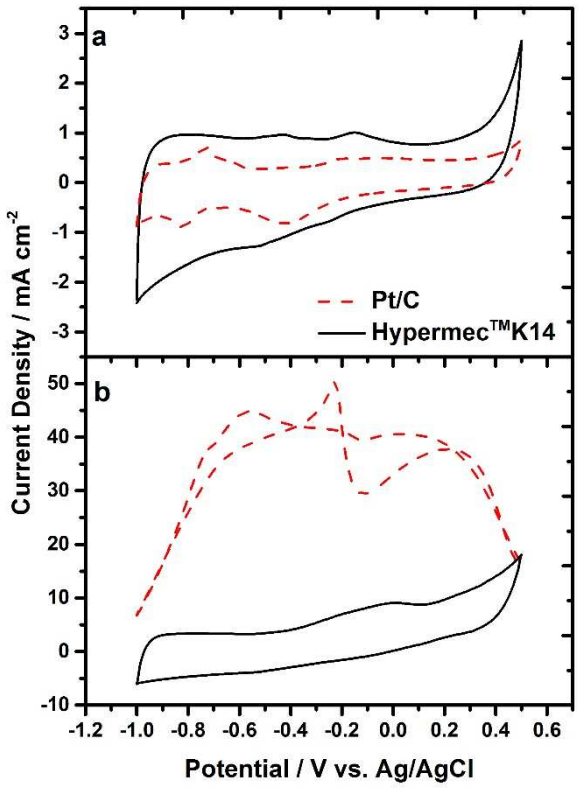

Figure 8. Cyclic voltammograms of Hypermec^{TM}K14 and 10 wt. % Pt/C catalysts in 2M KOH (a) and 2M KOH + 50mM $NaBH_4$ (b).

Electrochemical impedance spectroscopy (EIS) study of Passive DBFCs

AC impedance spectroscopy is a direct method for the study of various electrochemical processes involved in the operation of fuel cell. Herein, EIS was employed under various cell potentials, 0.2V, 0.5V and 0.7V, in order to investigate the impedance of both MEAs with more details. As shown in Figure 9, there are three arcs shown in each Nyquist spectrum for MEA-K14. The intercept on the real-axis at the high frequency is Rs, which is responsible for ohmic resistance. The first high-frequency component was not varied by changing the cell potential. Therefore, this region could not be associated to Faradic process or mass transport limitations of the MEA. This can probably be attributed to the internal ohmic resistance and granular electrode structure. The arc at medium frequencies can be ascribed to the charge transfer resistance, which can be recognized by the fact that it is varied with potential. The arc at low frequencies is related to the ion transfer from the cathode surface to the membrane.[35]

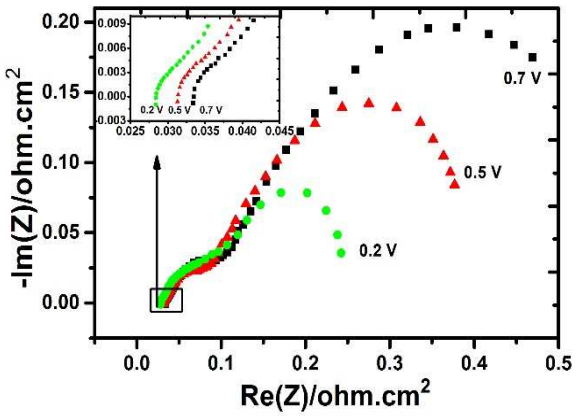

Figure 9. Nyquest spectra of Hypermec^{TM}K14 in air-breathing passive DBFC fueled with 3 wt. % SBH at 0.2V, 0.5V and 0.7V.

The effect of SBH concentrations, 1, 3, 5 and 8 wt. %, on the Nyquist spectrums of MEA-K14 was investigated as shown in Figure 10. As can be seen, mass transfer arc was decreased with increasing SBH from 1 wt. % to 5 wt. %. However, further increase in SBH up to 8 wt. % generated an extremely high level of hydrogen bubbles by borohydride hydrolysis on the anode surface, causing an increase in the Rs by the enhancement of the contact resistance. Indeed, the mobility of the carrier ions is decreased by increasing the fuel solution viscosity.[36]

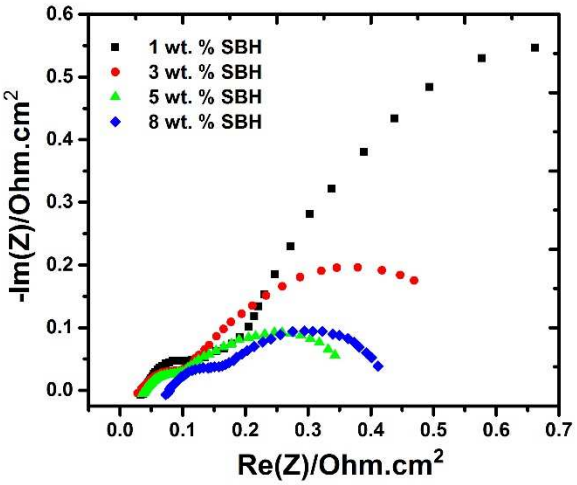

Figure 10. Nyquest spectra of Hypermec^{TM}K14 in air-breathing passive DBFC fueled with solution containing 1, 3, 5, and 8 wt. % of SBH.

Nyquist plots of two MEAs in SBH 5 wt. % and under different cell potentials, (0.2V, 0.5V and 0.7V) are shown in Figure 11 (a-c). It can be clearly seen that the MEA-Pt has higher ion and charge transfer resistances than MEA-K14, in a good agreement with the power density obtained by polarization curves. The present work raised intriguing research topics for future studies such as detailed EIS of the DBFC and determination of the number of electrons involved in the oxidation per BH_4^- anion on the Hypermec^{TM}K14 and explanation of the reaction intermediates and reaction pathways.

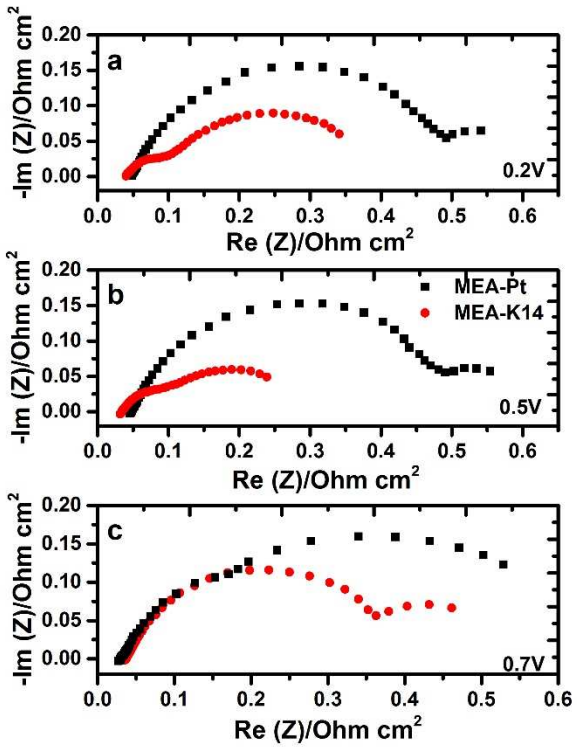

Figure 11. Comparison between Nyquest spectra of Hypermec^{TM}K14 and 10 wt. % Pt/C in air-breathing passive DBFCs fueled with 5 wt. % SBH at (a) 0.2 V (b) 0.5 V (c) 0.7 V.

Active direct borohydride fuel cell characterization

The performance of the Hypermec^{TM}K14 and 10 wt. % Pt/C cathodes was also compared in an active DBFC polarization experiments as well. The following results were recorded in active mode using peristaltic pumps for the fuel solution.
The fuel consisted of a borohydride solution containing 5 wt. % $NaBH_4$ in 10 wt. % NaOH and the oxidant consisted of gaseous oxygen. The flow rates for anolyte and oxidant were 6 and 500 mL min^{-1}, respectively. The temperatures used during fuel cell performance testing were 25 °C, 45 and 75 °C.
Figure 12 shows the performance of the active mode DBFC. As shown in Figure 12, a significant performance improvement was observed when the fuel cell temperature increased from 25 °C to 75 °C in active DBFC with Hypermec^{TM}K14 as cathodic catalyst due to improvements in electrode kinetics, ionic conductivity and the open circuit voltage. Moreover, the peak power density of the active DBFC with Hypermec^{TM}K14 as cathodic catalyst reached 890 mWcm^{-2} at 75 °C.
The comparison of DBFCs performances using different anode and cathode electrocatalysts in literature were summarized in Table 3. Comparing the results in Table 3, power output of DBFC using Hypermec^{TM}K14 as a cathode catalyst is very high in both passive and active mode.

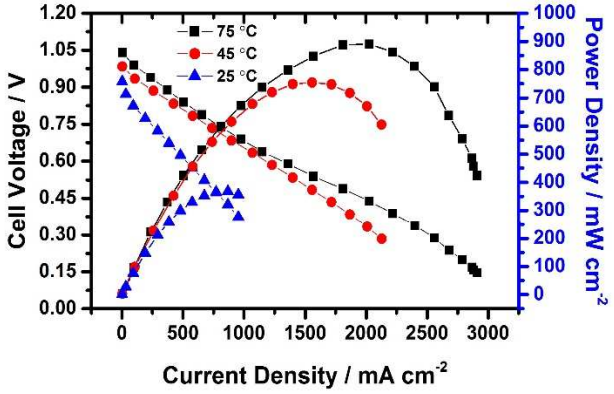

Figure 12. The performance of the active DBFC equipped by Hypermec^{TM}K14 under following conditions; oxidant: O_2, 20 kPa, 250 ml min^{-1}; Fuel: 5 wt. % of

Experimental

Preparation of membrane electrode assembly

A homemade passive direct borohydride single cell with the geometrical area of 5 cm^2 was employed in order to evaluate the characteristics of both catalysts, Fe-Co Hypermec^{TM}K14 (Acta S.P.A) and 10 wt. % Pt/C (Electrochem Co.) in the cathode side. Anode was prepared by the catalyst-coated substrate method onto a piece of the porous Ni foam support in order to make two identical anodes.22 The anode catalyst paste was prepared by mixing the 10 wt. % Pd/C (Sigma-Aldrich) and 5 wt. % polytetrafluoroethylene (PTFE), isopropyl alcohol (Merck) and deionized water and, finally dried at 60 ºC for 30 min under vacuum. The catalyst loading in the anode electrodes was 4.0 mg cm^{-2}. Two cathodes were prepared in the same way by coating catalysts slurry including Hypermec^{TM}K14 and 10 wt. % Pt/C onto a piece of hydrophobic carbon cloth (E-TEK). 10 wt. % PTFE was used as the binder in cathode catalyst ink. Catalyst loading in both electrodes was 1.7 mg cm^{-2}. An anion-exchange membrane A-006 (OH-form, Tokuyama membrane from Acta SpA) was used as the electrolyte.
Two MEAs were prepared and assembled in passive DBFC; one with a Fe-Co Hypermec^{TM}K14cathode catalyst denoted as MEA- K14 and the other with a 10 wt. % Pt/C cathode catalyst represented by MEA-Pt.

Morphological and physical characterization

The microstructure and morphology of the cathode electrodes were investigated using Hitachi S4160 (Japan) and JEOL-JSM-6360 SEM operating at an accelerating potential of 25 kV.

BET specific surface area measurements were performed using a NANO SORD instrument.

Electrochemical characterization

All electrochemical experiments were conducted in a passive DBFC using alkaline fuel containing 1, 3, 5 and 8 wt. % sodium borohydride (purity 99%, Merck), and 10 wt. % KOH (purity 99.99%, Merck) at the anode side and air in the cathode side after cell conditioning. All MEA needs to be activated in order to guarantee a stable performance.[37] For cell conditioning, reactants were introduced to the anode and cathode for a while of time under constant current density (100 mA cm^{-2}) until cell voltage reach to a constant and stable value. Before each loading cycle, cell was kept for 15 min in open circuit voltage and then two polarization curves were achieved.

Polarization curves

The DBFCs performance was evaluated using a Scribner test station (model 850e). Separated anode and cathode polarization curves were collected using a Zn/ZnO pseudo-reference electrode. The potential of Zn in 10 wt. % KOH vs. RHE is -524 mV. Each Polarization curve was obtained by scanning the cell voltage from OCV to 0.1V with a scan rate of 5 mV s^{-1}.

Borohydride tolerance measurement

The borohydride tolerance (electrocatalytic sensitivity to borohydride oxidation) of the electrocatalysts can be characterized directly in DBFC by the driven-cell mode technique. The measurements were performed by employing an electrochemical analyzer (Sama) and a single DBFC. A Zn/ZnO was employed as a pseudo-reference electrode. All of the driven-cell mode measurements were carried out between -0.524 and 0.524 V (vs. RHE) with a scan rate of 10 mV s^{-1} in a 10 wt. % KOH solution containing 1, 3, 5 and 8 wt. % of sodium borohydride at room temperature. During the driven-cell mode measurements, the cathode was deoxygenated via a nitrogen purge.

Activity measurement

The electrochemical activities of the catalysts were evaluated using cyclic voltammetry technique in a three electrodic compartment. A piece of Pt was used as the counter electrode and a saturated Ag/AgCl was used as the reference electrode. The ink-type working electrode was prepared as follows: 8 mg of the catalyst was ultrasonically mixed with 1 mL 80:20 isopropyl alcohol: water and 0.1 ml Nafion solution (5 wt. %, Dupont), forming a homogeneous ink. The ink was then pipetted onto a pre-treated glassy carbon (1mm in diameter, 0.0314 cm^2 geometrical area) electrode and dried at room temperature.
The CV measurements were carried out between -1 and 0.5 V (vs. Ag/AgCl) at a scan rate of 20 mV s^{-1} in a 2M KOH solution at 25 °C, whereas the current densities were normalized to the weight of the catalysts.

Electrochemical impedance spectroscopy

Impedance analysis was performed over a frequency range of 0.1 kHz and 10 kHz by Scribner test station (model 850e), at 0.2V, 0.5V and 0.7V with the amplitude of 5 mV.

Conclusions

In this work, an air breathing alkaline direct borohydride fuel cell based on the non-Pt cathode catalyst, Fe-Co Hypermec^{TM}K14, was constructed and evaluated in different fuel concentrations by i-V curves and EIS techniques. Morphological characterization, performance and BH_4^--tolerance of Hypermec^{TM}K14 cathode catalyst were investigated and compared to the 10 wt. % Pt/C in an air breathing alkaline DBFC.
Results demonstrated that Hypermec^{TM}K14 is an active nano-catalyst which can be used as a cathode catalyst in alkaline media. It is less sensitive toward electrooxidation of the SBH that crossed over from the anode side to the cathode side; therefore, higher OCV can be achieved by it, 0.970 V vs. 0.752 V compared to 10 wt. % Pt/C.
Driven-cell mode test results also proved that Hypermec^{TM}K14 has an excellent tolerance to electrooxidation of $NaBH_4$, at least one order of magnitude greater than 10 wt. % Pt/C.
Lower mass transfer and charge transfer resistances were obtained by EIS in a DBFC equipped with Hypermec^{TM}K14. The higher performance of Hypermec^{TM}K14, compared to 10 wt. % Pt/C, was explained on the basis of the properties of high surface transition metals and their remarkable activity and selectivity for oxygen reduction in alkaline solution. Therefore, passive DBFCs using Hypermec^{TM}K14 cathode catalyst are expected to give an acceptable performance for portable applications such as portable charger based on DBFC.

Acknowledgements

This work was carried out in Electrochemical Laboratory of Isfahan University of Technology (IUT). The authors would like to thanks the research council of IUT. We gratefully acknowledge the financial support of INSF through the project No.: 92006864 and the support of fuel cell steering committee and Iranian nano technology initiative council.
Furthermore, we would like to thank much more Paolo Bert and Alessandro Tampucci, Hubert A. Gasteiger, Claudio Bianchini, and Xiaoming Ren for their scholarly contributions in the development of Pt free catalyst.

Notes

[a] Department of Chemistry, Isfahan University of Technology, Isfahan 84156-83111, Iran
Tel.: +98 311 3913263
Fax: +98 311 3913263
E-mail address: m_zhiani@cc.iut.ac.ir (M. Zhiani).
URL: http://zhiani.iut.ac.ir

Table 3. The comparison of the active and passive DBFCs performance with different anode and cathode catalysts.

Cathode (catalyst loading / $mgcm^{-2}$)	Anode (catalyst loading / $mgcm^{-2}$)	Temp. /°C	Membrane	Oxidant (flow/ ml min^{-1})	Fuel concentration & flow ($mlmin^{-1}$)	Power/ $mWcm^{-2}$	Ref.
Eu_2O_3	$La_{0.88}Ce_{0.35}Pr_{0.03}Nd_{0.1}Ni_{5.2}CoMn_{0.41}Al_{0.42}$	RT	membraneless	Air-passive	1M NaOH-1M SBH (0.4)	66.4	[17]
MnO_2 (3)	PtRu (1)	RT	PVA/HAP	Air-passive	4MKOH-1MKBH_4 passive	45	[38]
CoPc (7.5)	$MmNi_{3.55}Co_{0.75}Mn_{0.4}Al_{0.3}$(150)	RT	Membraneless	Air-passive	6M KOH-0.8M K BH_4^- passive	90	[19]
$LaCoO_3$(7.5)	$MmNi_{3.55}Co_{0.75}Mn_{0.4}Al_{0.3}$(150)	RT	Membraneless	Air-passive	6M KOH-0.8M K BH_4^- passive	65	[23]
CeO2 (7)	$La_{0.88}Ce_{0.35}Pr_{0.03}Nd_{0.1}Ni_{5.2}CoMn_{0.41}Al_{0.42}$ (100)	20	Membraneless	O_2-passive	6M KOH-1M K BH_4^- passive	69.6	[39]
Sm2O3 (7)	$La_{0.88}Ce_{0.35}Pr_{0.03}Nd_{0.1}Ni_{5.2}CoMn_{0.41}Al_{0.42}$ (100)	20	Membraneless	O_2-passive	6M KOH-1M K BH_4^- passive	76.2	[39]
FePc (10)	($MmNi_{3.55}Co_{0.75}Mn_{0.4}Al_0.3$ (150)	RT	Membraneless	Air-passive	6M KOH-0.8M K BH_4^- passive	92	[20]
Pd/C (1_{Pt})	$La_{10.5}Ce_{4.3}Pr_{0.5}Nd_{1.4}Ni_{60.0}Co_{12.7}Mn_{5.9}Al_{4.7}$ (30)	RT	PHME+NME	2.5M H_2O_2-1.5M H_2SO_4-passive	7M NaOH-1.7M SBH- passive	81	[40]
MnO_2 (3)	PtRu (1)	RT	PVA/HAP	Air-passive	4M KOH-1M KBH_4 passive	45	[38]
Hypermec^{TM}(1.7)	Pd/C (4)	**RT**	**AEM**	**Air- Passive**	**10%NaOH-5% SBH passive**	**138**	**Current study**
Pt/C (1.7)	Pd/C	**RT**	**AEM**	**Air- Passive**	**10%NaOH-5% SBH passive**	**48**	**Current study**
RuO_2 (7.5)	CoO (75)	20	NRE-211	O_2 (5) Active	6M KOH-0.8M K SBH	243	[41]
Co(OH)2-PPY-C(10)	$Co(OH)_2$-C (10)	RT	Nafion 117	O_2 (150) Active	10%NaOH-5% SBH (5) Active	83	[42]
Co-PPY-C (1.2_{Co})	Ni-Pd/C-Zr-Ni(10)	RT	Nafion 117	O_2 (150) Active	10%NaOH-5% SBH (10) Active	65	[21]
Pt/C (0.3)	Pd/C (0.3)	25	Nafion 117	Air (150) Active	20%NaOH-1M SBH+TU (2) Active	15.1	[43]
AgNW/BP (5)	Ni-Pd/C (10)	25	Nafion 117	O_2 (150) Active	10%NaOH-5% SBH (10) Active	49	[44]
Pt/C (0.30)	Pd/C (1.08)	25	Nafion-117	Air (30) Active	20% NaOH-1.0M SBH (2) Active	19.4	[45]
Pt /C (1)	Pt–Ru/C (1)	30	ADP	O_2 (2.78) Active	1M NaOH-1M SBH (0.4) Active	78	[46]
Pt/C (1_{Pt})	Ni-Pd/C (5)	30	cross-linked chitosan	O_2 (150) Active	10%NaOH-5% SBH (5) Active	187	[47]
Hypermec^{TM}(1.7)	Pd/C (4)	**25**	**AEM**	**O_2(250) Active**	**10%NaOH-5% SBH (6) Active**	**368**	**Current study**
Pt/C (NA)	AuPt/C (1)	40	Nafion 112	O_2 (100) Active	2M NaOH-1M SBH (0.5) Active	112	[48]
Hypermec^{TM}(1.7)	Pd/C (4)	**45**	**AEM**	**O_2(250) Active**	**10%NaOH-5% SBH (6) Active**	**754**	**Current study**
Pt black (4)	Os/AvCarb^{TM} P75 (1.7)	60	Nafion 117	O_2 (1250) Active	2M NaOH-0.5M SBH (10) Active	75.9	[49]
Pt/C (1_{pt})	Ni_{37}–Pt_3/C (1)	60	Nafion 212	O_2 (100) Active	10%NaOH-5% SBH (1) Active	221.0	[50]
Pt/C (1_{Pt})	Ni-Pd/C (1_{metal})	60	PHME	O_2 (150) Active	10%NaOH-5% SBH (5) Active	242	[51]
Pt/C (1_{Pt})	Ni-Pd/C (5)	60	CsTP	O_2 (150) Active	10%NaOH-5% SBH (5) Active	685	[52]
Pt/C (1_{Pt})	Ni-Pd/C (5)	60	Nafion 112	O_2 (150) Active	10%NaOH-5% SBH (5) Active	270	[53]
$LaNiO_3$ (7.5)	CoO (70)	65	PFM	O_2 (5) Active	6M KOH–0.8M KBH4 (20) Active	663	[54]
Pt/C (0.5_{Pt})	$Pd_{50}Cu_{50}$/C (0.5)	68	Nafion 115	O_2 (200) Active	6M NaOH-1M SBH (3) Active	98	[1]
Pt/C	Ni-Pd/C (5)	70	ICCSHME	O_2 (150) Active	10%NaOH-5% SBH (5) Active	810	[55]
Co(OH)2-PPY-C(5)	Ni–Pt/C (10)	80	Nafion 117	O_2 (150) Active	10%NaOH-5% SBH (50) Active	550	[56]
FeTMPP (2_{metal})	Au/C (2_{Au})	85	Nafion 117	O_2 (200) Active	2.5M KOH–1.3M KBH_4 (10) Active	55.8	[18]
Pt/C (2_{Pt})	Au/C (2_{Pt})	85	Nafion 117	O_2 (200) Active	10%NaOH-5% SBH (10) Active	72.2	[57]
Hypermec^{TM}(1.7)	Pd/C (4)	**75**	**AEM**	**O_2(250) Active**	**10%NaOH-5% SBH (6) Active**	**890**	**Current study**

References

1. G. Behmenyar and A. N. Akın, *Journal of Power Sources*, 2014, 249, 239-246.
2. J. Ma, Y. Liu, Y. Liu, Y. Yan and P. Zhang, *Fuel Cells*, 2008, 8, 394-398.
3. F. Pei, Y. Wang, X. Wang, P. Y. He, L. Liu, Y. Xu and H. Wang, *Fuel Cells*, 2011, 11, 595-602.
4. Y. Wang, P. He and H. Zhou, *Energy & Environmental Science*, 2010, 3, 1515-1518.
5. D. Zhang, G. Wang, K. Cheng, J. Huang, P. Yan and D. Cao, *Journal of Power Sources*, 2014, 245, 482-486.
6. H. Cheng, K. Scott and K. Lovell, *Fuel Cells*, 2006, 6, 367-375.
7. D. A. Finkelstein, N. D. Mota, J. L. Cohen and H. D. Abruña, *The Journal of Physical Chemistry C*, 2009, 113, 19700-19712.
8. D. A. Finkelstein, C. D. Letcher, D. J. Jones, L. M. Sandberg, D. J. Watts and H. D. Abruña, *The Journal of Physical Chemistry C*, 2013, 117, 1571-1581.
9. A. C. Garcia, F. H. B. Lima, E. A. Ticianelli and M. Chatenet, *Journal of Power Sources*, 2013, 222, 305-312.
10. S. Özkar and M. Zahmakıran, *Journal of Alloys and Compounds*, 2005, 404–406, 728-731.
11. Z. Wang, L. Xin, X. Zhao, Y. Qiu, Z. Zhang, O. A. Baturina and W. Li, *Renewable Energy*, 2014, 62, 556-562.
12. G. Rostamikia and M. J. Janik, *Electrochimica Acta*, 2010, 55, 1175-1183.
13. B. H. Liu, Z. P. Li, K. Arai and S. Suda, *Electrochimica Acta*, 2005, 50, 3719-3725.
14. X. Wei, X. Yang, S. Li, Y. Chen and Y. Liu, *Electrochimica Acta*, 2011, 56, 7523-7529.
15. I. Merino-Jiménez, C. Ponce de León, A. A. Shah and F. C. Walsh, *Journal of Power Sources*, 2012, 219, 339-357.
16. Y.-g. Wang and Y.-y. Xia, *Electrochemistry Communications*, 2006, 8, 1775-1778.
17. X. Ni, Y. Wang, Y. L. Cao, X. P. Ai, H. X. Yang and M. Pan, *Electrochemistry Communications*, 2010, 12, 710-712.
18. H. Cheng and K. Scott, *Journal of Electroanalytical Chemistry*, 2006, 596, 117-123.
19. J. Ma, Y. Liu, P. Zhang and J. Wang, *Electrochemistry Communications*, 2008, 10, 100-102.
20. J. Ma, J. Wang and Y. Liu, *Journal of Power Sources*, 2007, 172, 220-224.
21. H. Y. Qin, Z. X. Liu, W. X. Yin, J. K. Zhu and Z. P. Li, *Journal of Power Sources*, 2008, 185, 909-912.
22. K. N. Zhu, H. Y. Qin, B. H. Liu and Z. P. Li, *Journal of Power Sources*, 2011, 196, 182-185.
23. Y. Liu, J. Ma, J. Lai and Y. Liu, *Journal of Alloys and Compounds*, 2009, 488, 204-207.
24. Y. Liu, Y. Liu, J. Ma and J. Lai, *Journal of Power Sources*, 2010, 195, 1854-1858.
25. G. Wang, Y. Bao, Y. Tian, J. Xia and D. Cao, *Journal of Power Sources*, 2010, 195, 6463-6467.
26. X. Yang, S. Li, Y. Liu, X. Wei and Y. Liu, *Journal of Power Sources*, 2011, 196, 4992-4995.
27. M. Zhiani, H. A. Gasteiger, M. Piana and S. Catanorchi, *International Journal of Hydrogen Energy*, 2011, 36, 5110-5116.
28. L. An, T. S. Zhao, S. Y. Shen, Q. X. Wu and R. Chen, *International Journal of Hydrogen Energy*, 2010, 35, 4329-4335.
29. C. Bianchini, V. Bambagioni, J. Filippi, A. Marchionni, F. Vizza, P. Bert and A. Tampucci, *Electrochemistry Communications*, 2009, 11, 1077-1080.
30. Y. S. Li, T. S. Zhao and Z. X. Liang, *Journal of Power Sources*, 2009, 187, 387-392.
31. W. Haijun, W. Cheng, L. Zhixiang and M. Zongqiang, *International Journal of Hydrogen Energy*, 2010, 35, 2648-2651.
32. H. Tributsch, *Electrochimica Acta*, 2007, 52, 2302-2316.
33. C. Ponce de León, F. C. Walsh, C. J. Patrissi, M. G. Medeiros, R. R. Bessette, R. W. Reeve, J. B. Lakeman, A. Rose and D. Browning, *Electrochemistry Communications*, 2008, 10, 1610-1613.
34. L. Yi, Y. Song, W. Yi, X. Wang, H. Wang, P. He and B. Hu, *International Journal of Hydrogen Energy*, 2011, 36, 11512-11518.
35. B. H. Liu and S. Suda, *Journal of Power Sources*, 2007, 164, 100-104.
36. C. Celik, F. G. B. San and H. I. Sarac, *Journal of Power Sources*, 2010, 195, 2599-2603.
37. V. B. Silva and A. Rouboa, *Fuel*, 2012, 93, 677-683.
38. C.-C. Yang, Y. J. Li, S.-J. Chiu, K.-T. Lee, W.-C. Chien and C.-A. Huang, *Journal of Power Sources*, 2008, 184, 95-98.
39. X. Ni, Y. Wang, F. Guo, P. Yao and M. Pan, *Journal of Rare Earths*, 2012, 30, 437-441.
40. N. A. Choudhury, Y. Sahai and R. G. Buchheit, *Electrochemistry Communications*, 2011, 13, 1-4.
41. X. Yang, X. Wei, C. Liu and Y. Liu, *Materials Chemistry and Physics*, 2014, 145, 269-273.
42. H. Y. Qin, Z. X. Liu, L. Q. Ye, J. K. Zhu and Z. P. Li, *Journal of Power Sources*, 2009, 192, 385-390.
43. C. Celik, F. G. Boyaci San and H. I. Sarac, *International Journal of Hydrogen Energy*, 2010, 35, 8678-8682.
44. H. Qin, L. Jiang, Y. He, J. Liu, K. Cao, J. Wang, Y. He, H. Ni, H. Chi and Z. Ji, *Journal of Materials Chemistry A*, 2013, 1, 15323-15328.
45. C. Celik, F. G. Boyaci San and H. I. Sarac, *Journal of Power Sources*, 2008, 185, 197-201.
46. N. Duteanu, G. Vlachogiannopoulos, M. R. Shivhare, E. H. Yu and K. Scott, *J Appl Electrochem*, 2007, 37, 1085-1091.
47. J. Ma, N. A. Choudhury, Y. Sahai and R. G. Buchheit, *Journal of Power Sources*, 2011, 196, 8257-8264.
48. X. Geng, H. Zhang, Y. Ma and H. Zhong, *Journal of Power Sources*, 2010, 195, 1583-1588.
49. V. W. S. Lam, D. C. W. Kannangara, A. Alfantazi and E. L. Gyenge, *Journal of Power Sources*, 2012, 212, 57-65.
50. X. Geng, H. Zhang, W. Ye, Y. Ma and H. Zhong, *Journal of Power Sources*, 2008, 185, 627-632.
51. J. Ma, N. A. Choudhury, Y. Sahai and R. G. Buchheit, *Fuel Cells*, 2011, 11, 603-610.
52. J. Ma, Y. Sahai and R. G. Buchheit, *Journal of Power Sources*, 2010, 195, 4709-4713.
53. J. Ma, Y. Sahai and R. G. Buchheit, *Journal of Power Sources*, 2012, 202, 18-27.
54. X. Yang, Y. Liu, S. Li, X. Wei, L. Wang and Y. Chen, *Sci. Rep.*, 2012, 2.
55. N. A. Choudhury, J. Ma and Y. Sahai, *Journal of Power Sources*, 2012, 210, 358-365.

56. H. Y. Qin, K. N. Zhu, L. Q. Ye and Z. P. Li, *Journal of Power Sources*, 2012, 208, 203-209.
57. H. Cheng and K. Scott, *Journal of Power Sources*, 2006, 160, 407-412.